

Interaction of Two Filament Channels of Different Chiralities

Navin Chandra Joshi¹, Boris Filippov², Brigitte Schmieder³, Tetsuya Magara^{1,4}, Young-Jae Moon^{1,4}, Wahab Uddin⁵

¹ *School of Space Research, Kyung Hee University, Yongin, Gyeonggi-Do, 446-701, Korea;
navin@khu.ac.kr, njoshi98@gmail.com*

² *Pushkov Institute of Terrestrial Magnetism, Ionosphere and Radio Wave Propagation of
the Russian Academy of Sciences (IZMIRAN), Troitsk, Moscow 142190, Russia*

³ *LESIA, Observatoire de Paris, PSL Research University, CNRS, Sorbonne Universités,
UPMC Univ. Paris 06, Univ. Paris Diderot, Sorbonne Paris Cité, 5 place Jules Janssen,
F-92195 Meudon, France*

⁴ *Department of Astronomy and Space Science, Kyung Hee University, Yongin,
Gyeonggi-Do, 446-701, Korea*

⁵ *Aryabhata Research Institute of Observational Sciences (ARIES), Manora Peak, Nainital
263 002, Uttarakhand, India*

ABSTRACT

We present observations of interactions between the two filament channels of different chiralities and associated dynamics that occurred during 2014 April 18 – 20. While two flux ropes of different helicity with parallel axial magnetic fields can only undergo a bounce interaction when they are brought together, the observations at the first glance show that the heated plasma is moving from one filament channel to the other. The *SDO*/AIA 171 Å observations and the PFSS magnetic field extrapolation reveal the presence of fan-spine magnetic configuration over the filament channels with a null point located above them. Three different events of filament activations, partial eruptions, and associated filament channel interactions have been observed. The activation initiated in one filament channel seems to propagate along the neighbor filament channel. We believe that the activation and partial eruption of the filaments bring the field lines of flux ropes containing them closer to the null point and trigger the magnetic reconnection between them and the fan-spine magnetic configuration. As a result, the hot plasma moves along the outer spine line toward the remote point. Utilizing the present observations, for the first time we have discussed how two different-chirality filament channels can interact and show interrelation.

Subject headings: Sun: activity - Sun: filaments, prominences - Sun: magnetic fields - magnetic reconnection

1. Introduction

Solar filaments/prominences are characterized as cool and dense structures that lie above the solar surface in the hot corona (Labrosse et al. 2010; Mackay et al. 2010). Filaments exist in the magnetic dips within magnetic configurations known as filament channels or flux ropes (Aulanier et al. 2002; Liu et al. 2012). Filaments and/or associated channels sometimes interact and show interesting dynamics in the chromosphere and low corona (Uralov et al. 2002; Schmieder et al. 2004; Su et al. 2007; Bone et al. 2009; Kumar et al. 2010; Chandra et al. 2011; Li & Ding 2012; Liu et al. 2010; Filippov 2011; Jiang et al. 2013; Jiang et al. 2014; Joshi et al. 2014). During interaction under some specific conditions, these magnetic structures can reconnect and change their foot point connectivity. They can also merge to form one common filament. The first type is known as ‘slingshot’ reconnection and the second type is ‘merging’ (see paper by Linton et al. (2001); Linton & Antiochos (2005)). Besides, large-scale flux-rope interaction/merging in the outer corona has also been observed in the form of CME-CME interaction and their merging (Gopalswamy et al. 2001; Joshi et al. 2013).

Some observational studies suggest the observational evidence of slingshot magnetic reconnection between filaments (Kumar et al. 2010; Chandra et al. 2011; Filippov 2011; Jiang et al. 2013). Kumar et al. (2010) and Chandra et al. (2011) first reported the interaction, reconnection, and footpoint connectivity change between two nearby filaments using $H\alpha$ observations on 2003 November 20. Later on, Filippov (2011) reported a few observational cases showing pairs of large filaments joining and exchanging their halves. More recently, Jiang et al. (2013) reported another observational evidence of partial slingshot reconnection during interaction of two filaments on 2011 December 3.

There are relatively few numerical simulations, which have been performed for the slingshot reconnection between flux ropes (Linton et al. 2001; Linton & Antiochos 2005; Török et al. 2011a). Linton et al. (2001) and Linton & Antiochos (2005) presented different types of flux rope interaction using three dimensional magnetohydrodynamic (MHD) simulations for convection zone conditions. Later on, Török et al. (2011a) simulated the 2003 November 20 filament interaction using a three dimensional zero β MHD model for coronal conditions and interpreted it in terms of ‘slingshot’ reconnection between two magnetic flux ropes.

Merging of two filament channels after dynamic interactions have also been observed by

Schmieder et al. (2004); Bone et al. (2009); Jiang et al. (2014); Joshi et al. (2014). Schmieder et al. (2004) found evidence of merging of two segments with dextral chiralities to form a long dextral filament. Recently, Jiang et al. (2014) reported the interaction and merging of two sinistral filaments on 2001 December 6 and found that they form a new long magnetic channel. More recently, Joshi et al. (2014) reported an interesting dynamic event of merging of two filament channels and formation of a long compound flux rope on 2014 January 1. On the basis of numerical simulations, some authors discussed various conditions necessary for interaction/merging of filaments. DeVore et al. (2005) and Aulanier et al. (2006) modeled filaments as differentially sheared arcades and found that two filaments, occupying a single polarity inversion line (PIL) in a bipolar large-scale magnetic configuration, easily merged if their chiralities were identical and axial magnetic fields were aligned. This is in accordance with empirical rules for filament interaction found by Martin et al. (1994) and Schmieder et al. (2004). However, in a quadrupolar configuration the situation is more complex and ambiguous (DeVore et al. 2005; Linton 2006; Romano et al. 2011).

Linton et al. (2001) and Linton & Antiochos (2005) analyzed numerically the reconnection of two twisted flux tubes contacting at different angles. The result of interaction depends on the twist handedness of the tubes and the angle between their axial magnetic fields. A pair of oppositely twisted flux tubes shows a bounce interaction, if their axial magnetic fields are parallel, and slingshot reconnection, if their axial magnetic fields are anti-parallel or perpendicular. Linton et al. (2001) and Linton & Antiochos (2005) considered isolated flux tubes without a surrounding magnetic field. But flux ropes containing filaments are not isolated flux tubes. They are imbedded into coronal magnetic fields created mostly by photospheric sources and follow basically photospheric PILs. For example, observations of filaments crossing each other at different heights are very rare. Oppositely twisted flux ropes with antiparallel axial magnetic fields need the presence of an additional PIL between them to be in equilibrium in the coronal magnetic field. Therefore, the slingshot interaction of filaments of different chiralities may be different.

In this paper, we present observations of interaction of two adjacent filament channels of different chirality associated with two adjacent PILs within a fan-spine configuration. This kind of dynamic interaction has not been discussed in detail before. We discuss the filament-channel interaction dynamics, the probable magnetic reconnection at a null point above them, different helical motions, and the apparent exchange of heated plasma between different filament channels. The structure of the paper is as follows: Section 2 deals with the description of the observational data set used in the paper. Morphology and magnetic structure of the filaments are discussed in Section 3. Different events of interactions and associated plasma dynamics are described in Section 4. In Section 5, we present an interpretation of the observed phenomenon in the light of filament flux-rope models and discussion.

Main results and conclusions are listed in Section 6.

2. Observations

We used Big Bear Solar Observatory (BBSO) and *National Solar Observatory* (NSO)/*Global Oscillation Network Group* (GONG) $H\alpha$ observations for the present study. The BBSO high resolution images are collected from archive <http://www.bbso.njit.edu/> are used to investigate the chiralities of the filaments. The GONG data are available in the data archive at <http://halpha.nso.edu/archive.html> with full-disk images in 6563 Å line. The images have spatial resolution of 1'' and a cadence of around 1 min (Harvey et al. 2011). The GONG $H\alpha$ observations are used to get the information about the filament activation and partial eruption dynamics. We also used data of the *Atmospheric Imaging Assembly* (AIA; Lemen et al. (2012)) instrument on board the *Solar Dynamics Observatory* (SDO). It observes the full disk of the Sun in ultra-violet (UV) and extreme ultra-violet (EUV) wavelengths with a minimum cadence of 12 s and a pixel size of 0.6''. We used AIA images in 304 and 171, 193, 131 and 94 Å wavelength channels. The line-of-sight (LOS) photospheric magnetic field data are obtained by the *Helioseismic and Magnetic Imager* (HMI; Schou et al. (2012)), with a spatial resolution of 1'' and a minimum cadence of 45 s. It is also an instrument on board *SDO*.

3. Morphological and Magnetic Structure of the Filaments

Figures 1(a) and 1(c) represent the BBSO $H\alpha$ images at $\sim 18:46$ UT on 2014 April 15 and $\sim 17:01$ UT on 2014 April 16, respectively. Figure 1(b) shows the *SDO*/AIA 304 Å images at $\sim 18:46$ UT on 2014 April 15. These images show the filaments and filament channels about 3-4 days before the first interaction that starts on 2014 April 18. Two dark filaments, named as the northern filament (NF) and southern filament (SF), are clearly seen in the $H\alpha$ image (Figures 1(a) and (c)). The extended filament channels of both filaments can be seen in the *SDO*/AIA 304 Å EUV image (Figure 1(b)). Figure 1(d) shows the *SDO*/HMI LOS magnetogram at 18:46:19 UT on 2014 April 15. To find out the filament positions and approximate endpoint locations, we tracked the filament spines from the $H\alpha$ image (see Figure 1(a)) and overplotted them in the LOS magnetogram (Figure 1(d)). NF/SF axis are shown by the red/orange colors, respectively in Figure 1(d). After comparing $H\alpha$, EUV 304 Å images, and the LOS magnetogram we determine that the eastern/western ends of both filaments are anchored in negative/positive polarity, respectively. Both filaments are stretched approximately from the south-east to the north-west along two different PILs.

The handedness or chirality of filaments can be determined using high-resolution $H\alpha$ images and the position of filament ends relative to the photospheric LOS magnetic fields. Figure 1(d) hints that the eastern ends of both filaments are anchored in negative polarities, while the western ends are rooted in positive polarities. In this case, the axial magnetic field in both filaments is directed from west to east. Accordingly, NF is sinistral, while SF is dextral because they are separated by positive polarity.

The $H\alpha$ images in Figures 1(a) and 1(c) also show that fine threads within NF and SF bodies deviated counterclockwise and clockwise from their axes, respectively. The filament barbs are left-bearing/ right-bearing for the NF/SF, which corresponds to sinistral chirality of NF and dextral chirality of SF (Martin et al. 1994; Martin 1998). Some of the visible barbs are marked with the red arrows in Figures 1(a) and 1(c).

The magnetic configuration surrounding the filaments can be deduced from the analysis of *SDO*/AIA 171 Å images (Figure 2) and the potential-field source-surface (PFSS) magnetic-field extrapolation (Schrijver & De Rosa 2003) (Figure 3). Figures 2(a)–(d) represent *SDO*/AIA 171 Å images at 10:48:59 UT on 2014 April 18 and at 00:36:11 UT, 10:28:59 UT, and 17:57:59 UT on 2014 April 19, respectively. To compare the coronal loop structure with a LOS magnetogram, we overplot positive (green) and negative (blue) LOS magnetic field contours on the AIA 171 Å image (Figure 2(a)). We clearly see arcades, connecting the central positive polarity with negative polarities on both sides, above the filaments. We also see long loops that connect the negative polarities to the remote region of positive polarity, near to the western endpoint of SF. All these images show the fan-spine configuration over the filaments. A null point is expected to be above the central positive polarity between the filaments. The outer spine field line emanates from the null point but is directed not radially into the outer corona, as it is usually assumed in fan-spine configurations, but deviates to the west and touches the photosphere near the western endpoint of SF within an area of positive polarity. This configuration is confirmed by the PFSS magnetic field extrapolation (Figure 3). To perform the PFSS extrapolation we used the PFSS software package available in IDL SolarSoftWare. Figure 3(a) shows the full disk magnetogram with extrapolated magnetic field lines, while the zoomed region corresponding to the black box is shown in Figure 3(b). The calculated field lines match quit well to the structure of coronal loops in *SDO*/AIA 171 Å images.

The filament channels were approaching each other from April 15 to April 18 as seen in *SDO*/AIA 304 Å images in Figure 4. The filament channels manifest themselves as long dark structures. They are quite separated on April 15 (Figure 4(a)), come slowly closer to each other during April 16-17 (Figure 4(b)-(c)), and become very close on April 18 (Figure 4(d)). The closing of the filament channels is marked by the white arrows in all the panels in

Figure 4.

4. Dynamic Interactions of the Filament Channels

We observed three events of filament channel interactions during 2014 April 18–20. In this section we describe the detail observation of these interaction dynamics in multiwavelength channels.

4.1. First Event of Interaction and Associated Dynamics

The sequence of the images showing the first event of interaction are represented in Figure 5. The left panel shows the *SDO*/AIA 304 Å images ((a)–(d)), while the right panel show the NSO/GONG H α images ((e)–(h)). In Figure 5(a), the *SDO*/AIA 304 Å image is overplotted with *SDO*/HMI LOS magnetogram contours. Green/blue contours show the positive/negative polarity regions, respectively. In Figure 5(a), we see two nearby filament channels. However, at the same time in the H α image only SF is visible (Figure 5(e)). The first event of interaction starts around 20:14 UT on 2014 April 18 with the activation of the middle part of SF. The initial activation area is shown by the small white circle in Figure 5(a). After the activation, the middle part of the filament partially erupts towards the north. The activated filament is seen in Figure 5(b). Along with the partial eruption we also see the counterclockwise rotation of filament threads around the long filament axis, if we observe it from the east end (see the AIA 304 Å animation associated with Figure 5). This counterclockwise rotation of the threads can be the manifestation of the redistribution of the twist along the flux rope due to its expansion and swelling during the activation (Parker 1974). Negative helicity of a flux rope corresponds to the dextral chirality of a filament in flux-rope models.

The partial failed eruption of SF seems to trigger reconnection at the magnetic null that lie above the filament channels. It is exhibited by EUV brightenings at several places on either side of both filament channels simultaneously with the partial eruption and helical motion. These bright regions are marked by the white circles in Figure 5(c). Such brightenings are believed to appear due to hits of the chromosphere by fast electrons and heated plasma from the region of reconnection. After the partial failed eruption the heated as well as cool material of SF moves along the axis towards the eastern and western ends of the filament (directions are shown by the arrows in Figure 5(d)). The two separate filament channels are still observed very close to each other at 20:46:07 UT. Apart from the chromospheric

brightenings, no influence of SF activation on NF was observed.

The distance–time plot of the hot plasma movement is presented in Figure 6(a). The rough trajectory along which the distance measurements was made is shown by dashed black line in Figure 5(c). We tracked a bright plasma blob that moves towards the western end of SF. The east-most point was used as a reference point for the distance measurements. For more accurate results, we repeated the measurements three times and the standard deviations was used as errors. The linear fit to these data points is used to estimate an average speed. It is evident that the hot plasma moved with the average speed of $\sim 40 \text{ km s}^{-1}$ between 20:25 and 20:50 UT.

4.2. Second Event of Interaction and Associated Dynamics

Figure 7 represents the selected *SDO*/AIA 304 Å and NSO/GONG H α images showing the second event of interaction and associated dynamics. Second event of interaction started at $\sim 15:33$ UT on 2014 April 19 with a compact brightening near the place of the closest approaching of the filament channels, just between them. Another small brightening appeared on the southern side of SF. The locations of these compact brightenings are marked by the white circles in Figure 7(a). The activation of NF started at $\sim 15:37$ UT near its eastern end (Figure 7(b)). At the same time, we also see a remote brightening (RB) on the west. The location of RB region is shown in Figure 7(b) with the white circle. Thereafter, the bright features propagate from the eastern end of NF to its middle part. The pattern of filament bright and dark threads looks like the upper part of a right-handed helix, which is consistent with the sinistral chirality of NF. What is most surprising, after reaching the place of the closest approaching of the filament channels the heated plasma propagates not to the north-west along the axis of the NF channel but to the west and south-west nearly along the axis of SF. At first glance, one might fancy that the eastern part of NF and the western part of SF form a joint magnetic structure allowing plasma to move easily from the eastern end of NF to the western end of SF. However, it is very doubtful if they can form such a structure because their chirality and helicity are opposite. We will discuss the problem in more detail in Section 5.

Signature of brightening around the magnetic null can also be seen in other AIA channels. Figure 8 shows the *SDO*/AIA 171, 193, 131 and 94 Å image at $\sim 15:41$ UT just after the partial filament eruption. We can see the brightening near the null point, which can be understood due to the magnetic reconnection there. The remote brightening signature is also visible in these channels.

The heated plasma first moves towards northwest direction with a speed of $\sim 90 \text{ km s}^{-1}$ and then towards southwest direction towards the western end of SF with a speed of $\sim 140 \text{ km s}^{-1}$. The kinematics of the plasma flows is shown in Figure 6(b). It represents the distance–time profiles of the plasma flows towards the north-west (red curve) and the south-west (green curve). The trajectories along which the northwest directed (white dashed line) and southwest directed (black dashed line) displacement measurements have been performed are shown in Figure 7(d). Two compact bright areas appeared on both sides of NF near its eastern end closer to the end of the second event (Figures 7(d), (g) and (h)). They can be considered as the compact ribbons formed by the partial eruption of the NF and the associated flare. The overplotted *SDO*/AIA 171 Å image at around $\sim 16:21$ UT shows the loop like structures joining the two bright ribbons and can be considered as the post flare loops.

4.3. Third Event of Interaction and Associated Dynamics

The third event in many features is similar to the second event of interaction. Figure 9 show the interaction dynamics in *SDO*/AIA 304 Å and NSO/GONO H α observations. It starts at $\sim 00:14$ UT on 2014 April 20 with brightenings near the place of the closest approaching of the filament channels and the southern side of SF. Immediately after that at $\sim 00:15$ UT we observe an activation and failed eruption of the eastern part of NF with formation of two bright ribbons on both sides of it. These ribbons can be formed as a result of reconnection between the legs of surrounding arcades during the partial eruption of the NF inside the northern arcades of the fan-spine structure. Soon after the activation, a remote brightening appears near the western end of SF at nearly the same place as in the second event (Figure 9(b), (e) and (f)). We also observed the brightening at the magnetic null point just after the partial eruption of NF in All the EUV channels (Figures 9(b) and 10). Figure 10 represents *SDO*/AIA 171, 193, 131 and 94 Å images at $\sim 00:18$ UT on 2014 April 20 also showing the brightening at the null. This brightening is due to some magnetic reconnection at the null point. The outer spine lines and the remote brightening can be seen in the hotter AIA channels (Figures 10(c) and (d)).

Heated plasma of the eastern part of NF forms a wide bright helical structure with intensive internal motions. Some part of the hot plasma moves from the middle of NF to the north-west along its axis to the western end, while a fraction of bright material moves to the western end of SF along the curved path nearly the same as in the second event. Different directions of plasma flows are shown by the arrows in Figure 9(c).

Several long threads as a whole shift from the northern side of the NF channel to the

southern side. This movement corresponds to clockwise rotation of a right-hand helix around its axis, as seen from the east, if the threads belong to its upper part and reveals untwisting of the helix. The eastern part of the helix looks more twisted, with threads more transversal to the axis. At the ending phase of the event, there are many blobs moving along the threads to the eastern end of NF. Their rotation (counterclockwise) is opposite to the rotation of the whole threads in the middle part of the helix because they presumably move along the upper part of the right-hand helix to its eastern end.

The distance–time profiles of these plasma motions are represented in Figure 11. Figure 11(a) shows the results for plasma moving to the north-west along the NF channel. We measured the profiles along two different trajectories shown by white dashed lines in Figure 9(d). Heated plasma moves with average speeds of ~ 110 and ~ 160 km s $^{-1}$ along trajectories 1 and 2, respectively. Figure 11(b) represents the profiles of plasma motion along the SF channel towards its western end. Since plasma moves along the curved path, we measured two profiles along straight lines, one for the northwestward motion and another for the southwestward motion. The speeds are ~ 90 and ~ 45 km s $^{-1}$, respectively.

5. Interpretation and Discussion

Two filaments gradually approach each other in their middle parts during their passage through the solar disk on 2014 April. We specify chiralities of the filament to be opposite. The NF fine structure definitely reveals the sinistral chirality, which is in accordance with the general hemispheric rule for the southern hemisphere. The chirality of SF is evident to be dextral for many reasons despite the violation of the hemispheric rule (see Section 3 and Figure 1 for more details). During several episodes from April 18 to April 20, the filaments show an activation and formation of a temporal structure that joins them into a united system. It looks puzzling because usually filaments with parallel axial magnetic fields and opposite chirality do not merge or reconnect with the formation of new stable or two different filaments from their halves.

In our interpretation of these observations we follow the flux-rope model (e.g., [Canou & Amari 2010](#); [Guo et al. 2010](#); [Joshi et al. 2014](#); [Filippov et al. 2015](#)) of filaments considering filament plasma accumulated in lower parts of helical flux tubes. Dextral filaments are contained within left-handed helices, while sinistral filaments fill right-handed ones. In our case, the axial magnetic fields of the two flux ropes are parallel but the azimuthal fields have different sense of rotation. Therefore, when these two flux ropes come close together side-by-side, both their axial and azimuthal field components have the same directions and cannot reconnect.

Two flux ropes of similar helicity either show merging or slingshot reconnection during their interaction (Linton et al. 2001; Török et al. 2011a). However, two flux ropes of different helicity with parallel axial magnetic fields can only undergo a bounce interaction (Linton et al. 2001) when they are brought together. They repulse from each other and cannot reconnect and form the joint structure. In our case, it is clear that SF/NF have dextral/sinistral chiralities, respectively with parallel axial magnetic fields. Therefore, the associated flux ropes should have different signs of twist, which is the condition for the bounce interaction.

We believe that although the events look like interaction of two filament channels, the most important interaction occurs between a flux rope and the surrounding coronal magnetic field of special structure. We clearly observe a fan-spine configuration of coronal loops over the filament channels, with a presumed null point above them (see Figure 2). The PFSS magnetic field extrapolation confirms the existence of the fan-spine magnetic configuration (see Figure 3).

The initial magnetic field-line distribution and subsequent plasma dynamics are shown in the schematic representation in Figure 12. The coronal structure is similar to a "pseudostreamer" (Wang et al. 2007; Rachmeler et al. 2014) with two flux ropes at the base. The left column represents the 3D disk view (Figure 12(a)), while the right column shows the projected view of selected 3D field lines (Figure 12(g)). However, in contrast to the "pseudostreamer" the outer spine field line emanating from the null point is not directed radially into the outer corona, but deviates to the west and touches the photosphere near to the endpoint of SF within an area of positive polarity (see Figures 2 and 3). In projection on the disk, the outer spine field line runs nearly parallel to the SF axis, so the plasma motion along the spine can easily be mixed up with the motion along the SF axis. We believe it is most probable in the observations of the filament interaction in our case.

In the first event the case is looking simple, i.e., reconnection between the inner green and the outer blue line (Figures 12(b), 12(h) and 5). However in the second and third case the scenario is little complex. There is no anti-parallel field lines belonging to flux ropes that contain SF and NF. But if each of the flux ropes approaches the null point, its azimuthal field can reconnect with outer field lines of the opposite lobe, i.e., circular field lines of the red flux rope can reconnect with the outer green line. This case seems to take place in the second (Figures 12(c), 12(i), and 7) and third (Figures 12(e), 12(k), and 9) events of the filament interaction. The locations of reconnections are shown by pink stars in Figure 12. Due to the projected view of 3D field lines in a 2D plan, the reconnected field lines appear as a single line in panels (j) and (l) of Figure 12. But actually it represents the two different sets of field lines as shown in 3D view (Figures 12(d) and 12(f)).

After the reconnection some amount of heated plasma confined previously within the flux rope is able to propagate along the field lines of the surrounding magnetic configuration. In particular, it can move along the spine and this motion mimics the movement along the SF axis. Penetration of the flux-rope plasma into the outer structure can be illustrated by a simple 2-D model.

Let us consider the coronal magnetic field with fan-spine structure as a sum of a vertical homogeneous magnetic field B_0 and a vertical 2-D dipole located at $x = 0$, $z = z_d$ with the dipole moment M . If y is the axis of translational symmetry, x is the horizontal axis and z is the vertical axis with the origin at the photospheric level, the external field is described by y -component of vector potential \mathbf{A}

$$A_y^e = B_0 x + \frac{Mx}{x^2 + (z - z_d)^2}. \quad (1)$$

We put into this field a flux rope in the simplest form of a straight linear current along the y -axis. According to the boundary condition for the coronal current I on the photosphere, its vector potential can be written as (van Tend & Kuperus 1978; Molodenskii & Filippov 1987; Filippov et al. 2001)

$$A_y^I = \frac{I}{c} [\ln((x - x_0)^2 + (z + z_0)^2) - \ln((x - x_0)^2 + (z - z_0)^2)], \quad (2)$$

where x_0 and z_0 are the coordinates of the coronal current. Neglecting the weight of the flux rope its equilibrium position (x_0, z_0) is defined by the equations:

$$B_0 - M \frac{x_0^2 - (z_0 - z_d)^2}{(x_0^2 + (z_0 - z_d)^2)^2} = 0, \quad (3)$$

$$\frac{I}{cz_0} - M \frac{2x_0(z_0 - z_d)}{(x_0^2 + (z_0 - z_d)^2)^2} = 0. \quad (4)$$

Figure 13(left) shows field lines described by Equations (1) and (2) for dimensionless parameters $B_0 = 1$, $M = -4$, $z_d = -1$, and the value of I/c being close to the critical value of the current I_c over which the stable equilibrium is impossible (Molodenskii & Filippov 1987; Filippov et al. 2001). Spaces between several magnetic surfaces $A_y = \text{const}$ are shadowed by different tints. Figure 13(right) shows the same magnetic surfaces for the slightly increased value of I_c . The magnetic flux Φ conservation between the current and the photosphere is taken into account in the form

$$\Phi = Mx_0 \left(\frac{1}{x_0^2 + (z_0 - z_d)^2} - \frac{1}{x_0^2 + z_d^2} \right) + \frac{I}{c} \ln \frac{2z_0}{r_0} = \text{const}, \quad (5)$$

where $r_0 = 0.01$ is the radius of a flux tube with nearly homogeneous current density, which should be taken into account to avoid divergency.

When the equilibrium position becomes higher, some of previously closed field lines reconnect with open field lines at the null point. Plasma (possibly previously heated) confined between some closed magnetic surfaces is able to propagate along the open field lines into the upper corona and to the photosphere. Such scenario we expect to happen in the present case of filament interactions during 2014 April 18 – 20.

The first event and reconnection on April 18 was initiated by the activation and partial eruption of SF that bring the inner green field lines toward the null point and trigger the reconnection (Figures 12(b) and 12(h)). The observed brightenings (shown by the chartreuse color) near the foot points of the fan lines on both sides of the filaments is strong evidence of the null point reconnection (Figure 5(c)). The accelerated electrons move after the reconnection towards the foot points of the fan lines and produce brightenings there. In the second event on April 19, the activation and partial eruption of NF bring its field lines to the magnetic null and trigger reconnection (Figures 12(c) and 12(i)). The brightening at the foot points of the fan lines was also observed in this event. Some part of the heated NF plasma travels along the outer spine over the SF towards the western foot point (Figures 12(d) and 12(j)). The third event on April 20 is quite similar to the second one with a partial eruption of NF again, but there is additional flow of heated NF plasma along the axis of NF towards the western end (along the white arrows in Figure 9(c)).

Apparent brightening near the null point has also been observed just after the partial eruption in both the second and third cases, which provides a signature of magnetic reconnection (see Figures 8 and 10). In *SDO/AIA* images the filaments and filament channels, arcades and loops look the same after second event. However, we believe that there should be some changes in the magnetic configuration as shown in panel(j) of Figure 12. The flux rope with helical field lines (black color) and the outer green spine lines reconnect (Figures 12(c) and 12(d)) and create a new domain between a few new reconnected lines joining the two systems (shown by dotted black lines in Figures 12(d) and 12(j)). We believe that a similar reconnection is occurring during the third event (Figure 12(e) and 12(k)). The activation of the filaments can be understood by some photospheric magnetic changes. Looking at the magnetic field evolution in this region, we note flux cancellation close to the eastern end of SF, emerging flux close to the middle and the western end of SF along with the expending motions (see the *SDO/HMI* animation attached with Figure 1). These motions could create shear and cancelling flux and be the trigger of the activation of the filaments. The SF

remains stable after the first event. From this we could guess that the twist of SF flux rope became less and the overlying arcades are more potential. On the other hand the NF being overlaid by less and more sheared arcades can rise and reach the null point.

6. Conclusions

In this paper, we discuss the observations of the interactions between two near-by filament channels of different chirality with parallel axial magnetic fields. We found a key role of the interaction of partially erupting filaments and associated flux ropes with the overlying fan-spine magnetic structure. On the basis of the analysis of coronal EUV images and magnetic field calculations, we come the following main results.

1. *SDO*/AIA EUV observations show close connection between two near-by filament channels during three episodes of activation and interaction of the filaments with different chiralities on 18, 19, and 20 April 2014, respectively.
2. The observations as well as the PFSS calculations clearly show the existence of fan-spine magnetic configuration over the two filaments.
3. Although the events look like interaction of two filament channels, the most important interaction occurs between the flux ropes containing the filaments and the surrounding coronal magnetic field of special structure. The activations and partial eruptions of the filaments are believed to be responsible for the reconnection between their magnetic field lines with the coronal field at the magnetic null that lies above them.

The most interesting aspect in these events is the geometry of the spine line of the coronal fan-spine structure. In projection on the solar disk, the spine line runs nearly parallel to the SF axis, close to it. The remote point, where the outer spine line is anchored in the photosphere, is located near the western end of SF. It leads to the wrong impression that plasma from one filament channel easily penetrates to the other filament channel with the opposite chirality. In fact, the filament plasma penetrates into the coronal structure and propagates along coronal field lines, which are located above the SF axis. We strongly believe that the activations and partial eruptions of both filaments were responsible for the reconnection at the magnetic null. Plasma of the filaments then moves along the spine line to the remote footpoint, which lies near the western end of SF.

Interaction of two nearby filament channels with different filament chiralities within large-scale coronal fan-spine magnetic structure have not been observed before, although

fan-spine configurations have been discussed in case of solar eruption in "pseudostreamers" (Wang et al. 2007; Török et al. 2011b; Rachmeler et al. 2014; Yang et al. 2015), jets (Pariat et al. 2009; Filippov et al. 2009, 2015) and flares (Wang et al. 2014; Joshi et al. 2015).

Observations of filament interactions and merging are crucial for better understanding of reconnection between large-scale coronal flux ropes. It also provide the information of interaction the flux ropes with the overlying magnetic configurations. These magnetic structures are responsible for different types of eruptions. High-resolution observations provide important inputs for the MHD modeling of flux-rope interactions and reconnections, which are needed to understand the physics of flux-rope dynamics more clearly.

The authors thank the referee for his/her valuable comments/suggestions. We thank SDO/AIA, SDO/HMI, BBSO and GONG/NSO teams for providing their data for the present study. This work is supported by the BK21 plus program through the National Research Foundation (NRF) funded by the Ministry of Education of Korea. NCJ thank School of Space Research, Kyung Hee University for providing Postdoctoral grant. We are thankful to Dr. Pascal Démoulin for his valuable suggestions.

REFERENCES

- Aulanier, G., DeVore, C. R., & Antiochos, S. K. 2002, *ApJ*, 567, L97
- Aulanier, G., DeVore, C. R., & Antiochos, S. K. 2006, *ApJ*, 646, 1349
- Bone, L. A., van Driel-Gesztelyi, L., Culhane, J. L., Aulanier, G., & Liewer, P. 2009, *Sol. Phys.*, 259, 31
- Canou, A., & Amari, T. 2010, *ApJ*, 715, 1566
- Chandra, R., Schmieder, B., Mandrini, C. H., Démoulin, P., Pariat, E., Török, T., & Uddin, W. 2011, *Sol. Phys.*, 269, 83
- DeVore, C. R., Antiochos, S. K., & Aulanier, G. 2005, *ApJ*, 629, 1122
- Filippov, B., Golub, L., & Koutchmy, S. 2009, *Sol. Phys.*, 254, 259
- Filippov, B., Martsenyuk, O., Srivastava, A. K., & Uddin, W. 2015, *Journal of Astrophysics and Astronomy*, 36, 157
- Filippov, B. P. 2011, *Astronomy Reports*, 55, 541

- Filippov, B. P., Gopalswamy, N., & Lozhechkin, A. V. 2001, *Sol. Phys.*, 203, 119
- Gopalswamy, N., Yashiro, S., Kaiser, M. L., Howard, R. A., & Bougeret, J.-L. 2001, *ApJ*, 548, L91
- Guo, Y., Schmieder, B., Démoulin, P., Wiegmann, T., Aulanier, G., Török, T., & Bommier, V. 2010, *ApJ*, 714, 343
- Harvey, J. W., et al. 2011, in *AAS/Solar Physics Division Abstracts #42*, 1745
- Jiang, Y., Hong, J., Yang, J., Bi, Y., Zheng, R., Yang, B., Li, H., & Yang, D. 2013, *ApJ*, 764, 68
- Jiang, Y., Yang, J., Wang, H., Ji, H., Liu, Y., Li, H., & Li, J. 2014, *The Astrophysical Journal*, 793, 14
- Joshi, N. C., Liu, C., Sun, X., Wang, H., Magara, T., & Moon, Y.-J. 2015, *ApJ*, 812, 50
- Joshi, N. C., Magara, T., & Inoue, S. 2014, *ArXiv e-prints*
- Joshi, N. C., Srivastava, A. K., Filippov, B., Kayshap, P., Uddin, W., Chandra, R., Prasad Choudhary, D., & Dwivedi, B. N. 2014, *ApJ*, 787, 11
- Joshi, N. C., et al. 2013, *Advances in Space Research*, 52, 1
- Kumar, P., Manoharan, P. K., & Uddin, W. 2010, *ApJ*, 710, 1195
- Labrosse, N., Heinzel, P., Vial, J.-C., Kucera, T., Parenti, S., Gunár, S., Schmieder, B., & Kilper, G. 2010, *Space Sci. Rev.*, 151, 243
- Lemen, J. R., et al. 2012, *Sol. Phys.*, 275, 17
- Li, Y., & Ding, M.-D. 2012, *Research in Astronomy and Astrophysics*, 12, 287
- Linton, M. G. 2006, *Journal of Geophysical Research (Space Physics)*, 111, 12
- Linton, M. G., & Antiochos, S. K. 2005, *ApJ*, 625, 506
- Linton, M. G., Dahlburg, R. B., & Antiochos, S. K. 2001, *ApJ*, 553, 905
- Liu, R., Kliem, B., Török, T., Liu, C., Titov, V. S., Lionello, R., Linker, J. A., & Wang, H. 2012, *ApJ*, 756, 59
- Liu, Y., Su, J., Shen, Y., & Yang, L. 2010, in *IAU Symposium, Vol. 264, IAU Symposium*, ed. A. G. Kosovichev, A. H. Andrei, & J.-P. Rozelot, 99

- Mackay, D. H., Karpen, J. T., Ballester, J. L., Schmieder, B., & Aulanier, G. 2010, *Space Sci. Rev.*, 151, 333
- Martin, S. F. 1998, *Sol. Phys.*, 182, 107
- Martin, S. F., Bilimoria, R., & Tracadas, P. W. 1994, in *NATO Advanced Science Institutes (ASI) Series C*, Vol. 433, *NATO Advanced Science Institutes (ASI) Series C*, ed. R. J. Rutten & C. J. Schrijver, 303
- Molodenskii, M. M., & Filippov, B. P. 1987, *Soviet Ast.*, 31, 564
- Pariat, E., Antiochos, S. K., & DeVore, C. R. 2009, *ApJ*, 691, 61
- Parker, E. N. 1974, *ApJ*, 191, 245
- Rachmeler, L. A., Platten, S. J., Bethge, C., Seaton, D. B., & Yeates, A. R. 2014, *ApJ*, 787, L3
- Romano, P., Pariat, E., Sicari, M., & Zuccarello, F. 2011, *A&A*, 525, A13
- Schmieder, B., Mein, N., Deng, Y., Dumitrache, C., Malherbe, J.-M., Staiger, J., & Deluca, E. E. 2004, *Sol. Phys.*, 223, 119
- Schou, J., et al. 2012, *Sol. Phys.*, 275, 229
- Schrijver, C. J., & De Rosa, M. L. 2003, *Sol. Phys.*, 212, 165
- Su, J., Liu, Y., Kurokawa, H., Mao, X., Yang, S., Zhang, H., & Wang, H. 2007, *Sol. Phys.*, 242, 53
- Török, T., Chandra, R., Pariat, E., Démoulin, P., Schmieder, B., Aulanier, G., Linton, M. G., & Mandrini, C. H. 2011a, *ApJ*, 728, 65
- Török, T., Panasenco, O., Titov, V. S., Mikić, Z., Reeves, K. K., Velli, M., Linker, J. A., & De Toma, G. 2011b, *ApJ*, 739, L63
- Uralov, A. M., Lesovoi, S. V., Zandanov, V. G., & Grechnev, V. V. 2002, *Sol. Phys.*, 208, 69
- van Tend, W., & Kuperus, M. 1978, *Sol. Phys.*, 59, 115
- Wang, H., Liu, C., Deng, N., Zeng, Z., Xu, Y., Jing, J., & Cao, W. 2014, *ApJ*, 781, L23
- Wang, Y.-M., Sheeley, N. R., Jr., & Rich, N. B. 2007, *ApJ*, 658, 1340
- Yang, J., Jiang, Y., Xu, Z., Bi, Y., & Hong, J. 2015, *ApJ*, 803, 68

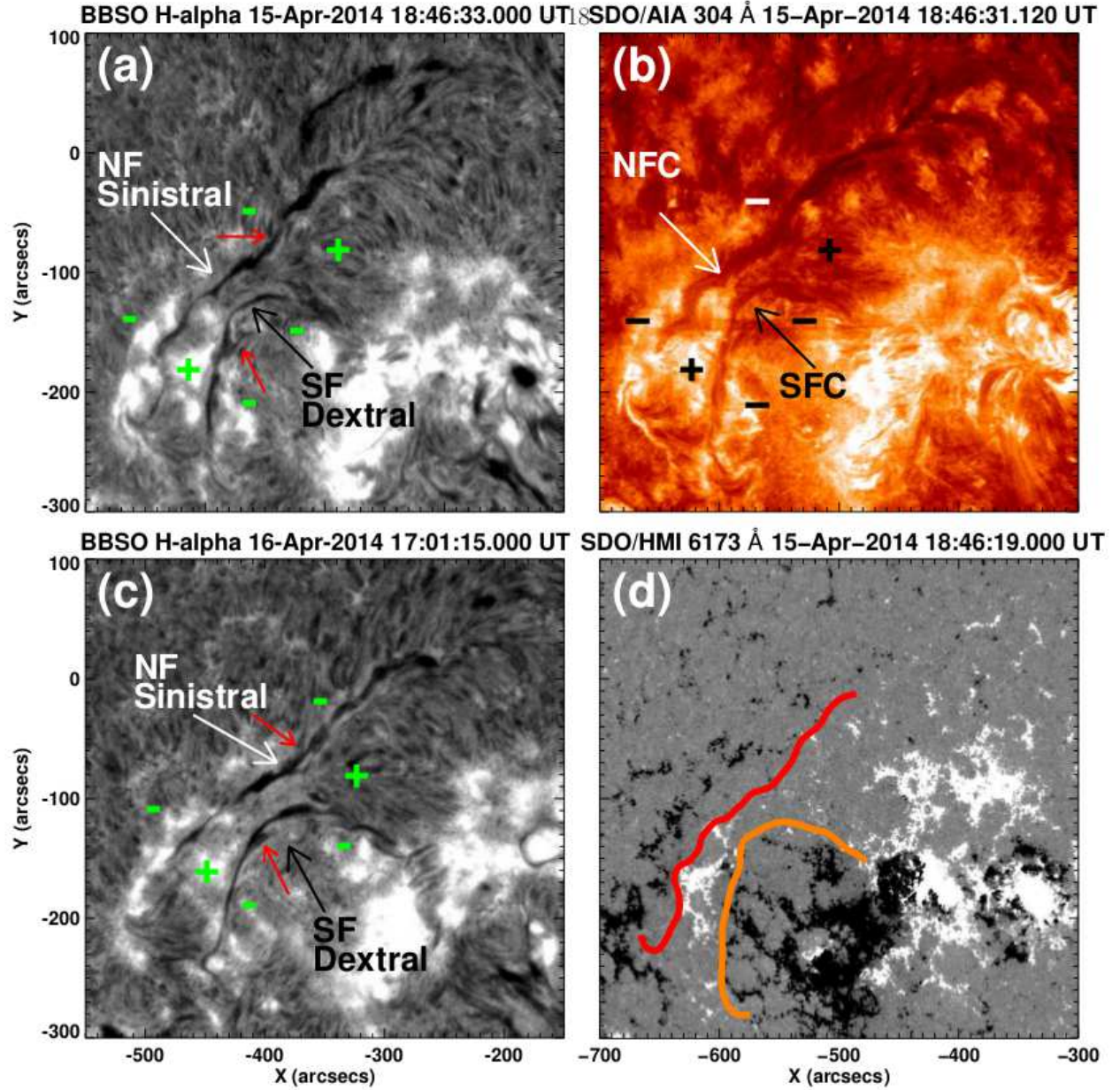


Fig. 1.— BBSO H α images at \sim 18:46 on 2014 April 15 (a) and \sim 17:01 UT on 2014 April 16 (c), showing the presence of northern (NF) and southern (SF) filaments. (b) *SDO*/AIA 304 Å images at \sim 18:46 UT on 2014 April 15. Northern filament channel (NFC) and southern filament channel (SFC) are shown in panel (b). The *SDO*/HMI line-of-sight magnetogram (d) with overplotted filament spines shown by red (NF) and orange (SF) colors. The filament spines are tracked from the H α image shown in panel (a).

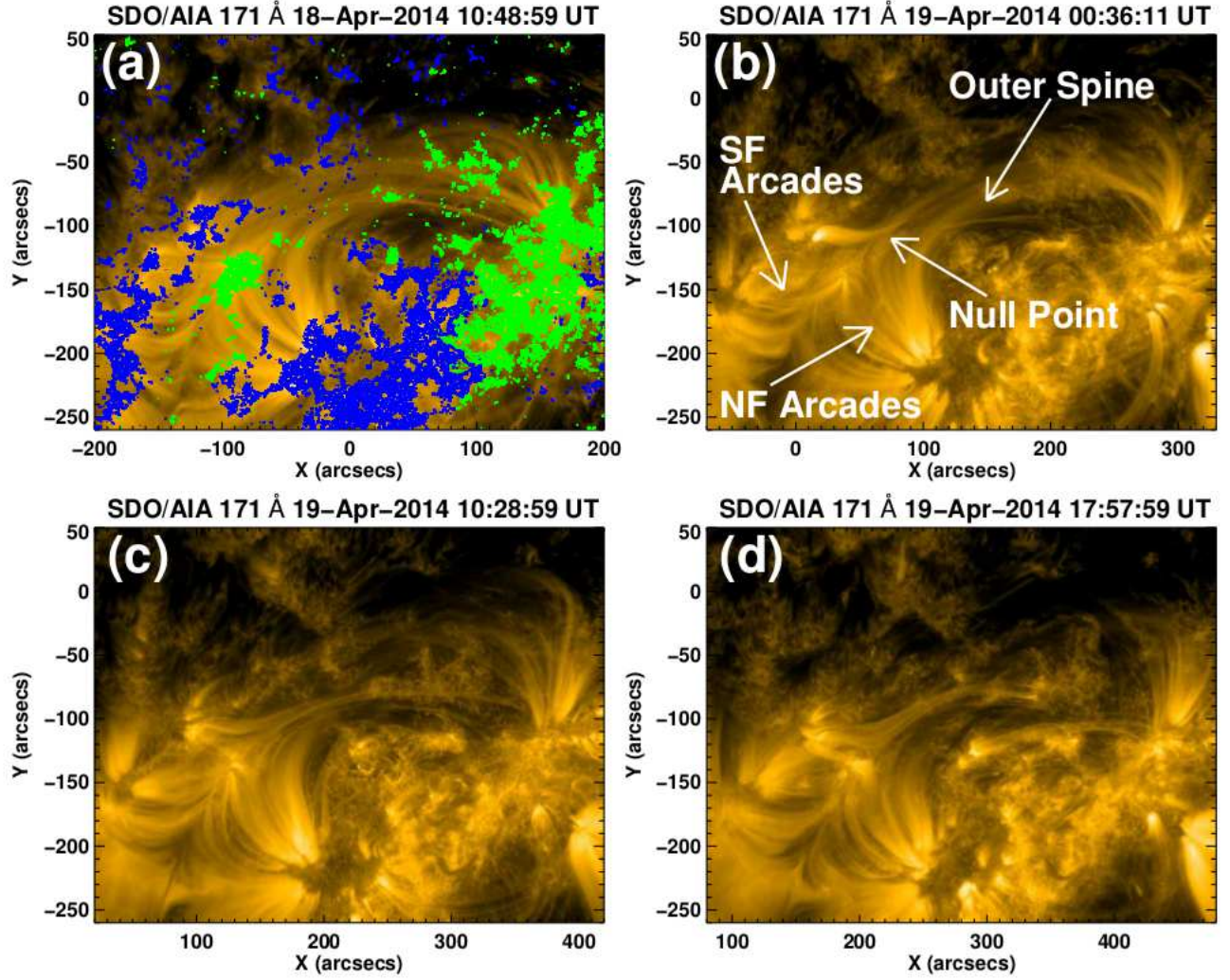


Fig. 2.— *SDO*/AIA 171 Å images on 2014 April 18–19 showing the fan-spine type configuration over two filament channels. The southern filament (SF) arcades, northern filament (NF) arcades, the approximate location of null point and the outer spine are marked in panel (b).

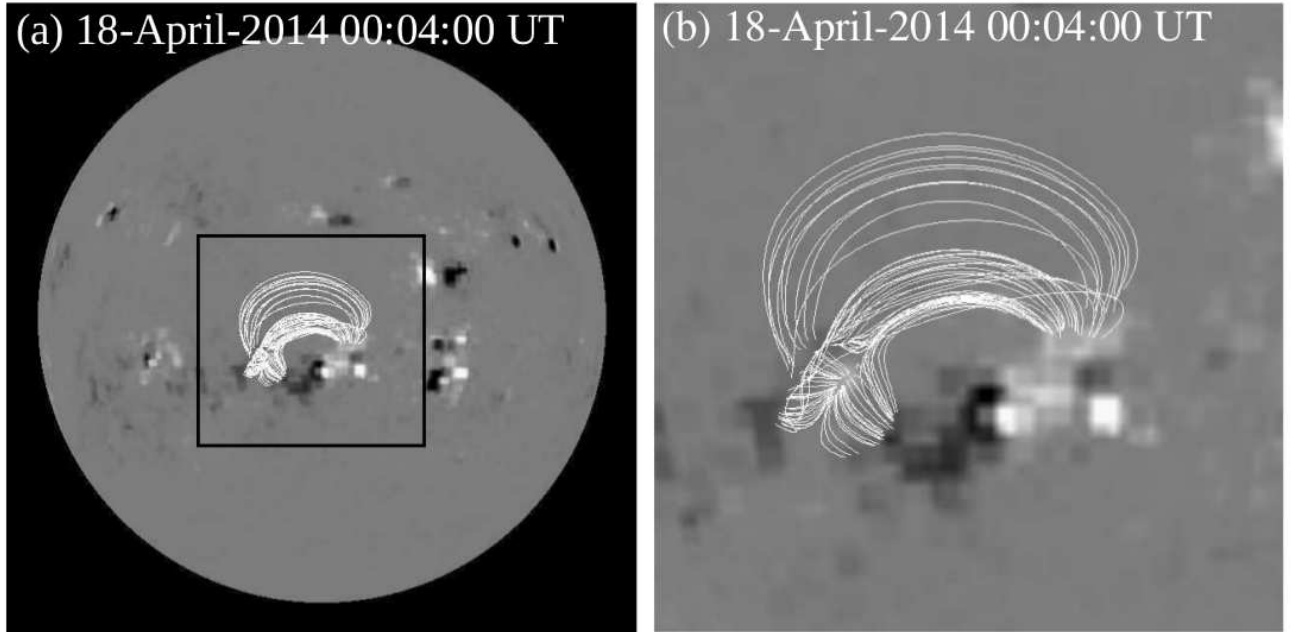


Fig. 3.— (a) PFSS magnetic field extrapolation showing a full disk view of the coronal magnetic field structure over the filaments. (b) The zoomed view corresponding to the black box shown in the panel (a).

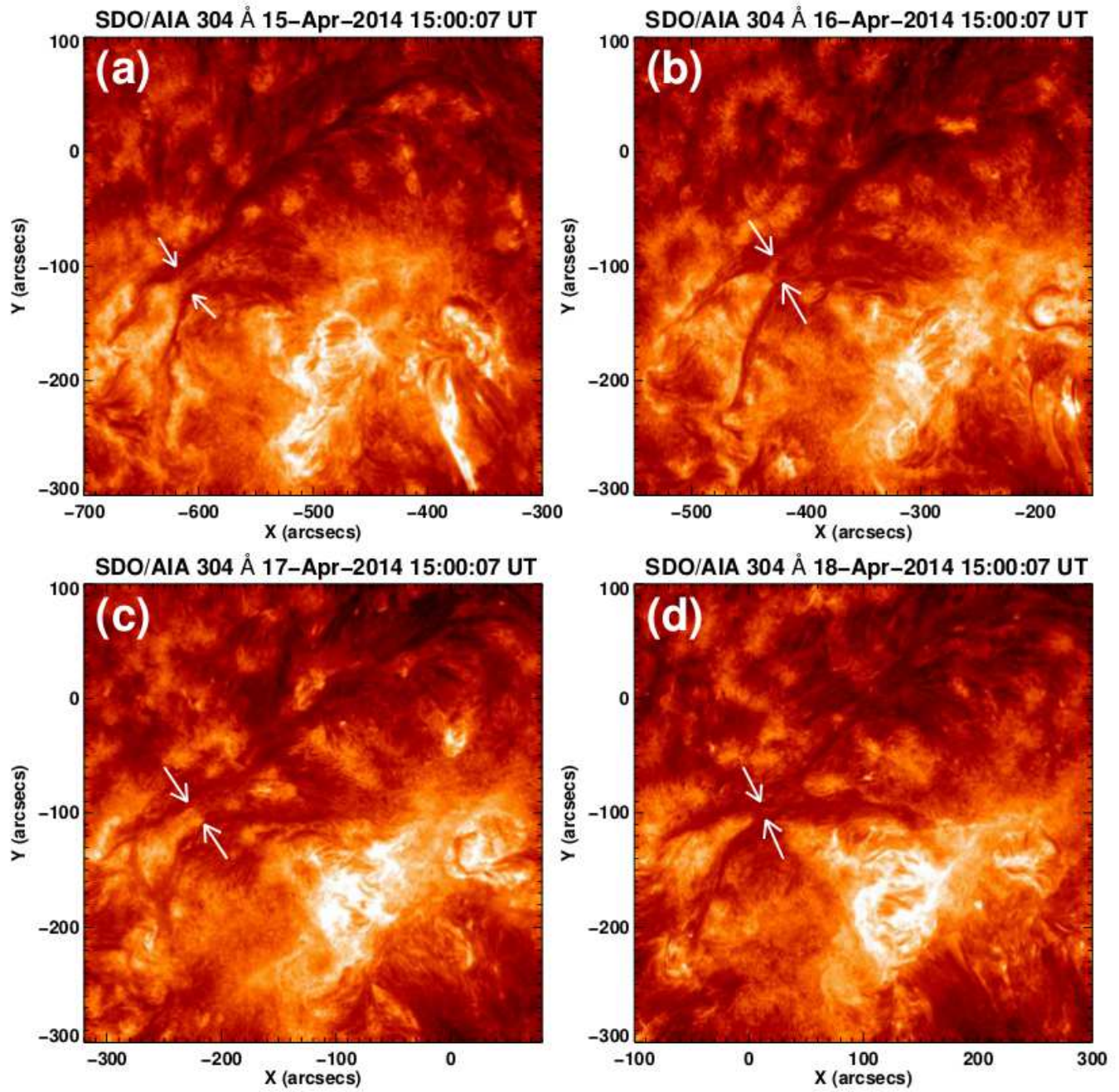


Fig. 4.— Evolution of filament channels during 2014 April 15–18 in *SDO*/AIA 304 Å images. Arrows show the closing in of filament channels.

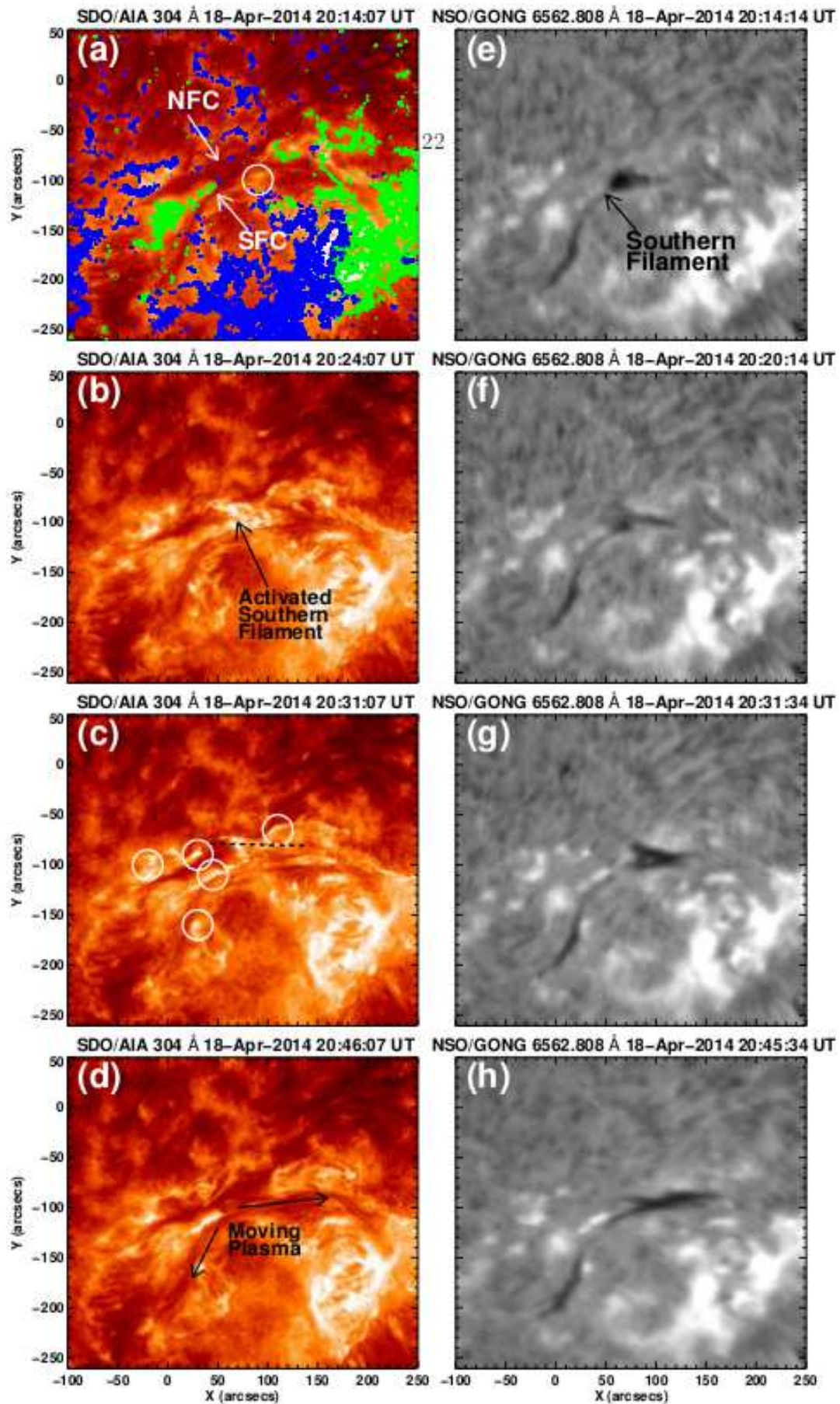


Fig. 5.— *SDO/AIA* 304 Å (left column) and the *NSO/GONG* H α (right column) images showing the first event of interaction/reconnection. Northern filament channel (NFC) and southern filament channel (SFC) are shown in panel (a).

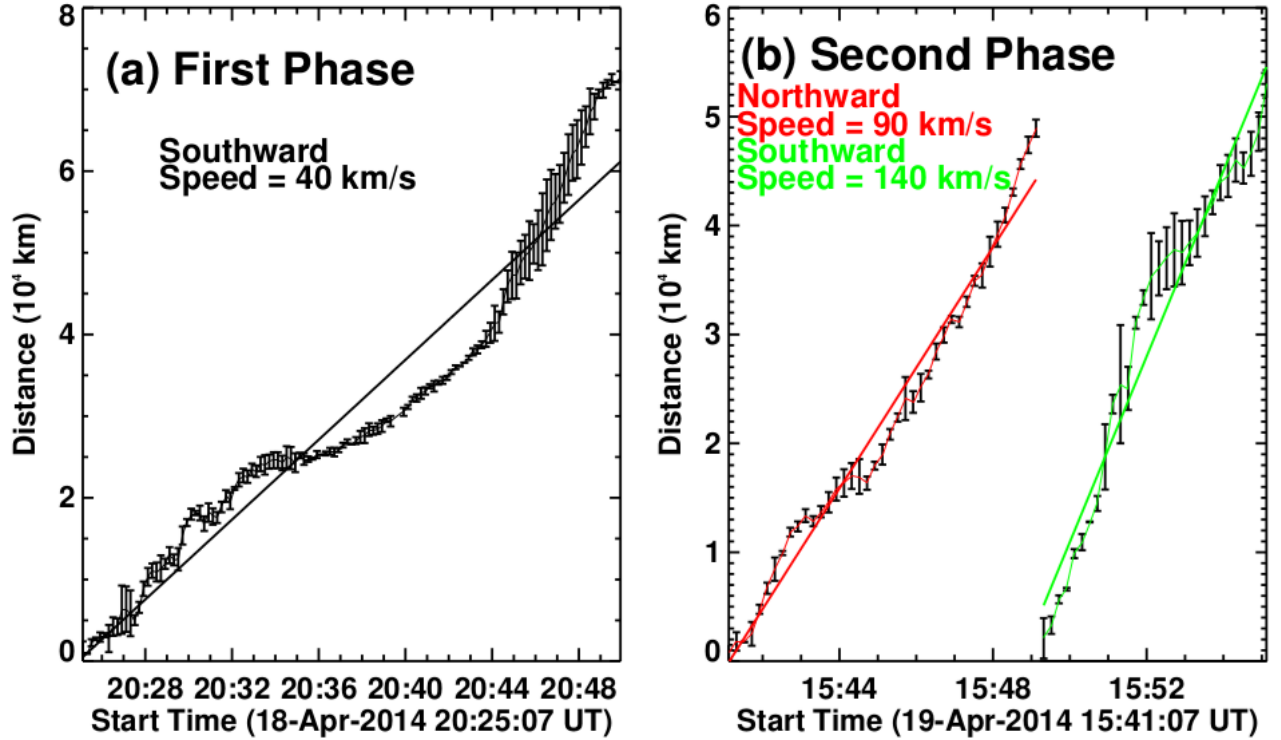


Fig. 6.— (a) Projected distance-time profile of the plasma flow along the trajectory shown by the dashed black line in Figure 5(c) measured using *SDO*/AIA 304 Å images. (b) The same for the trajectories shown by the dashed white (in red color) and black lines (by green color) in Figure 7(d). The error bars are the standard deviations estimated using three repeated measurements of the same value. The linear fit method has been used to estimate the average speeds.

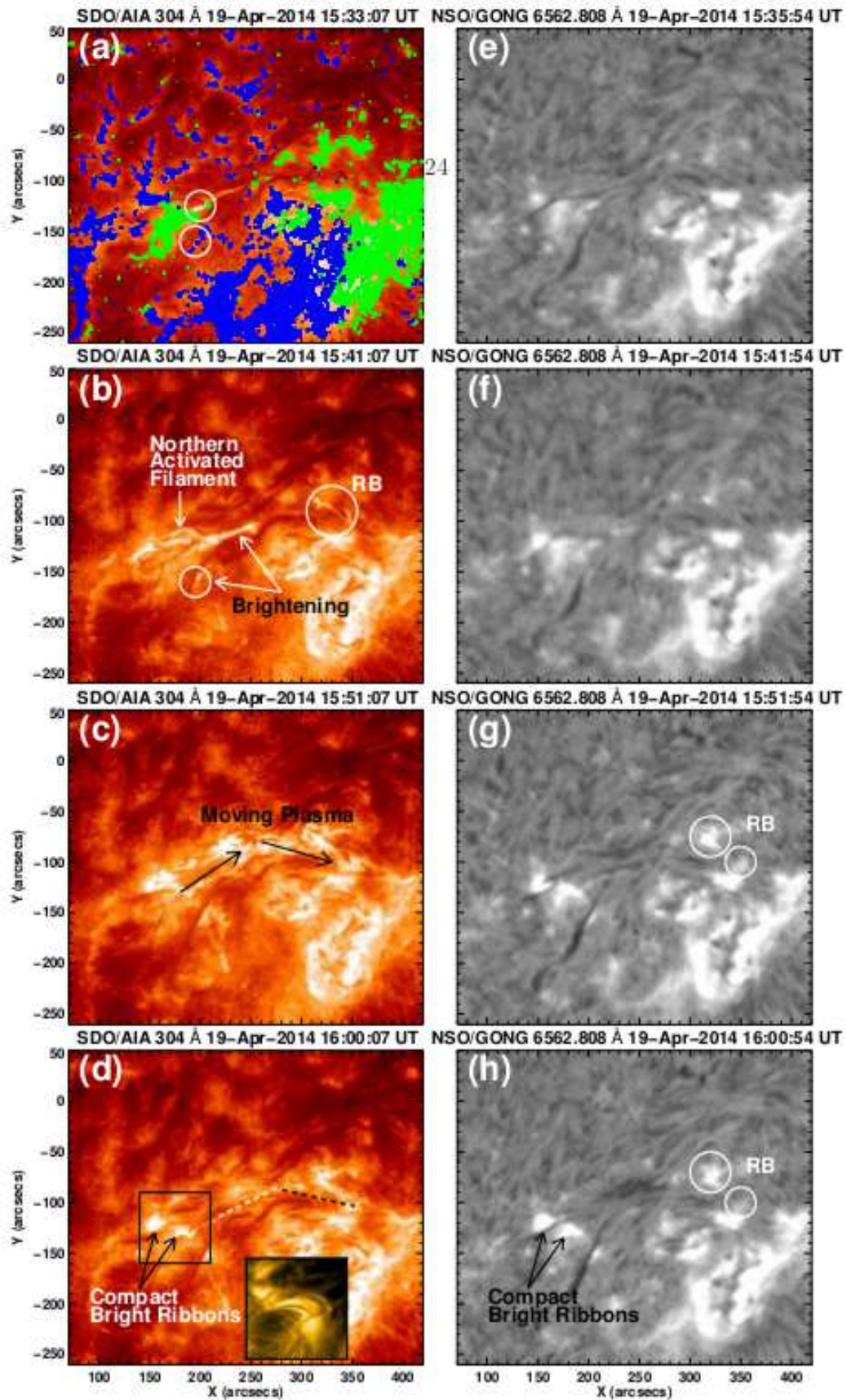


Fig. 7.— *SDO*/AIA 304 Å (left column) and the NSO/GONG H α (right column) images showing the second event of interaction/reconnection. The inset image over panel (d) is SDO/AIA 171 Å image at \sim 16:21 UT on 2014 April 19, showing the post flare loops joining the two compact bright ribbons. Remote brightening regions are shown by white circles in panels (b), (g) and (h).

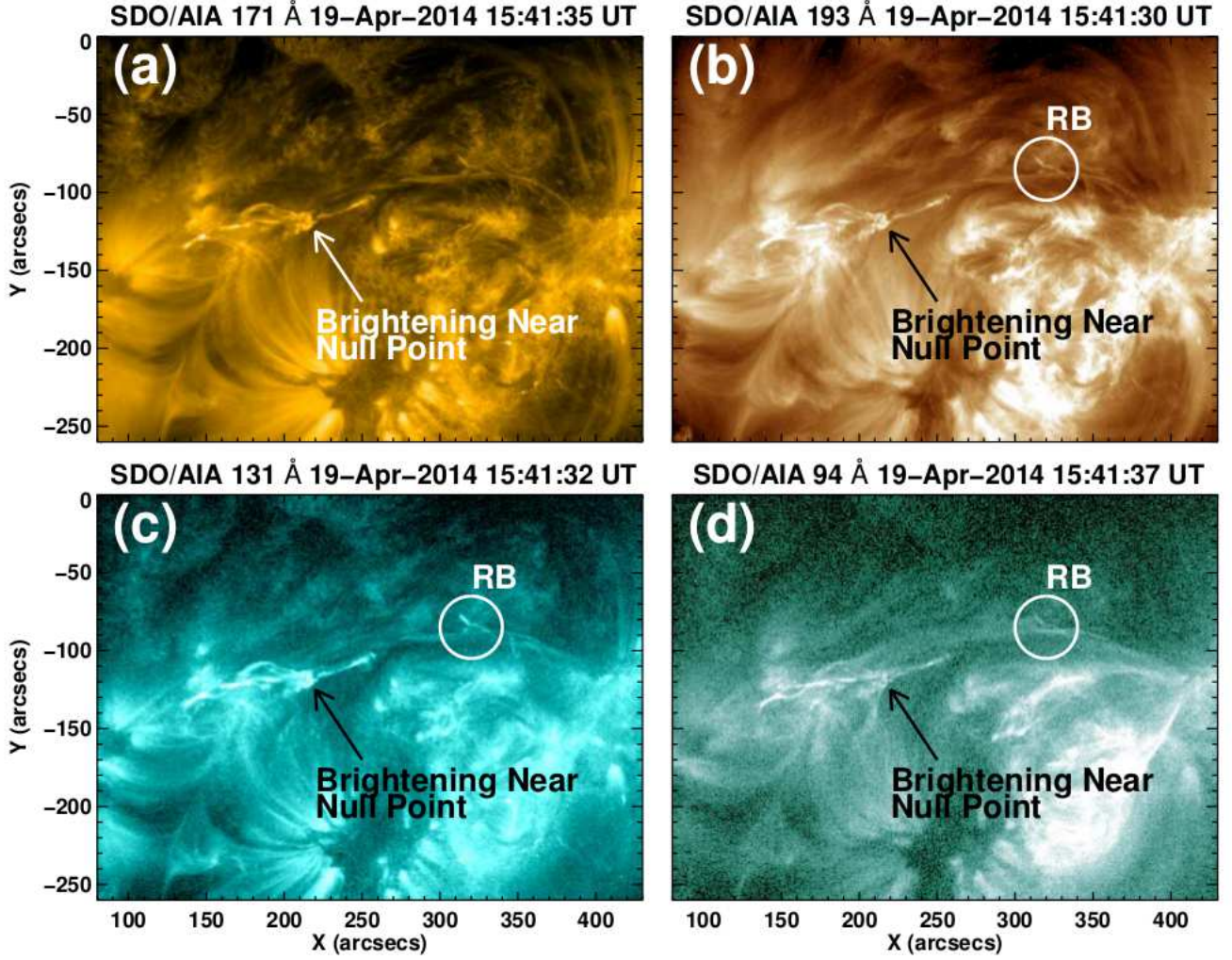


Fig. 8.— *SDO/AIA* 171 (a), 193 (b), 131 (c), 94 (d) Å images at $\sim 15:41$ UT on 2014 April 19 showing the brightening near the magnetic null point and the appearance of remote brightening (RB). The RB area are marked with a white circle in panels (b), (c) and (d).

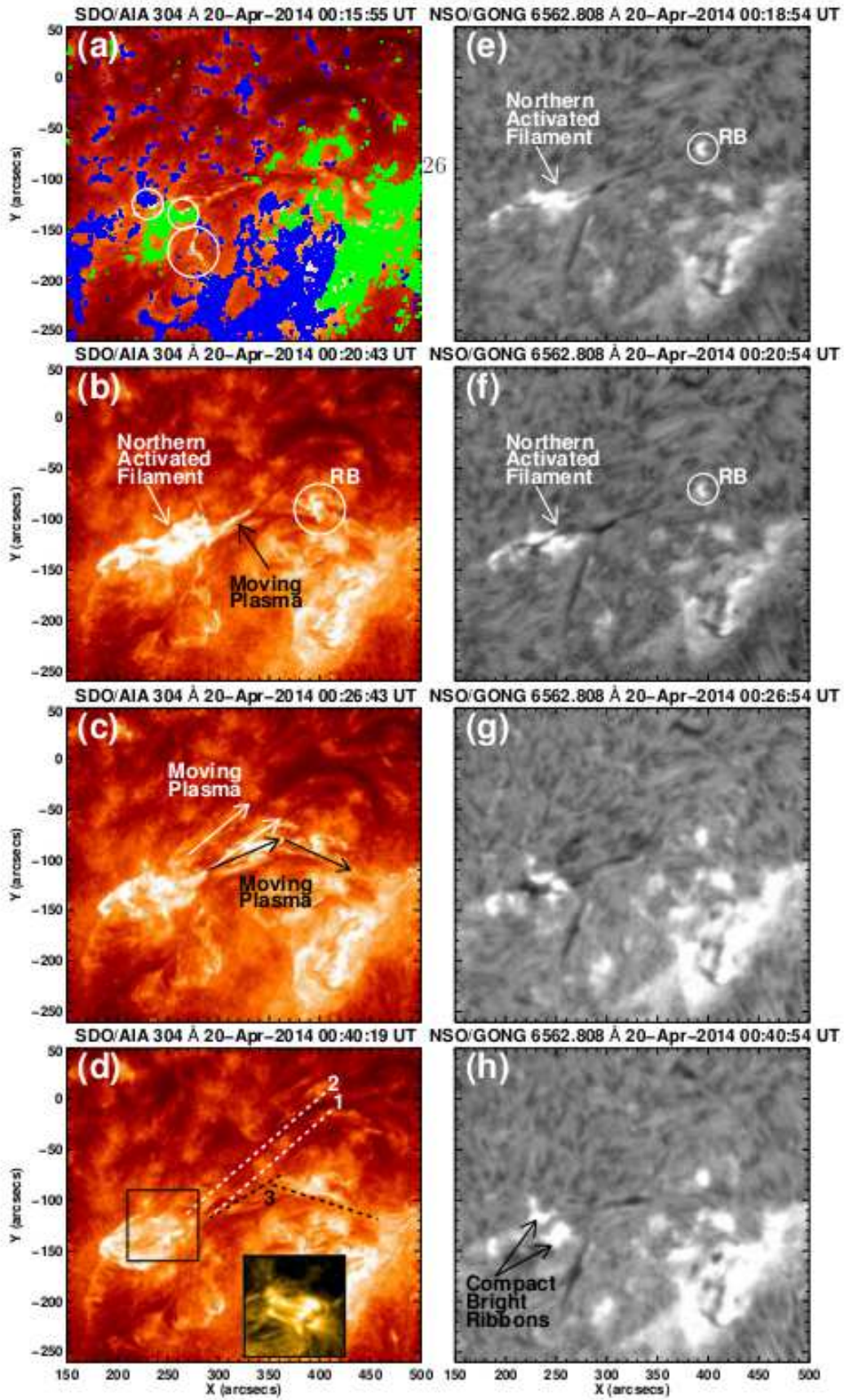


Fig. 9.— *SDO*/AIA 304 Å (left column) and the *NSO*/GONG H α (right column) images showing the third event of interaction/reconnection. The inset image over panel (d) is *SDO*/AIA 171 Å image at \sim 00:40 UT on 2014 April 20, showing the post flare loops joining the two compact bright ribbons (panels g and h). Remote brightening regions are shown by white circles in panels (b), (e) and (f).

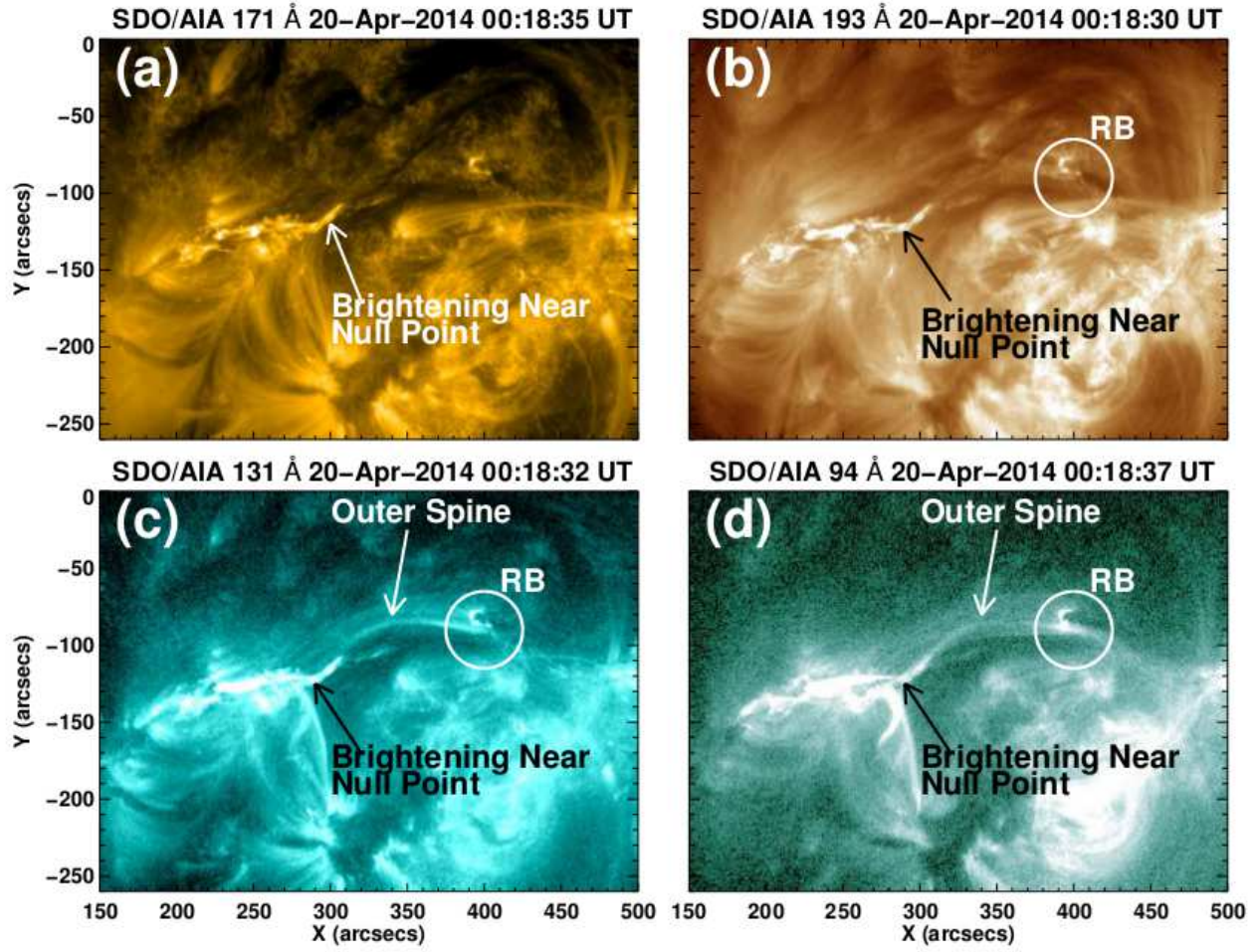


Fig. 10.— *SDO/AIA* 171 (a), 193 (b), 131 (c), 94 (d) Å images at $\sim 00:18$ UT on 2014 April 20 showing the brightening near the magnetic null point and the appearance of remote brightening (RB) and outer spine. The RB area are shown by white circle in panels (b)–(d), while the outer spine are represented in panels (c) and (d).

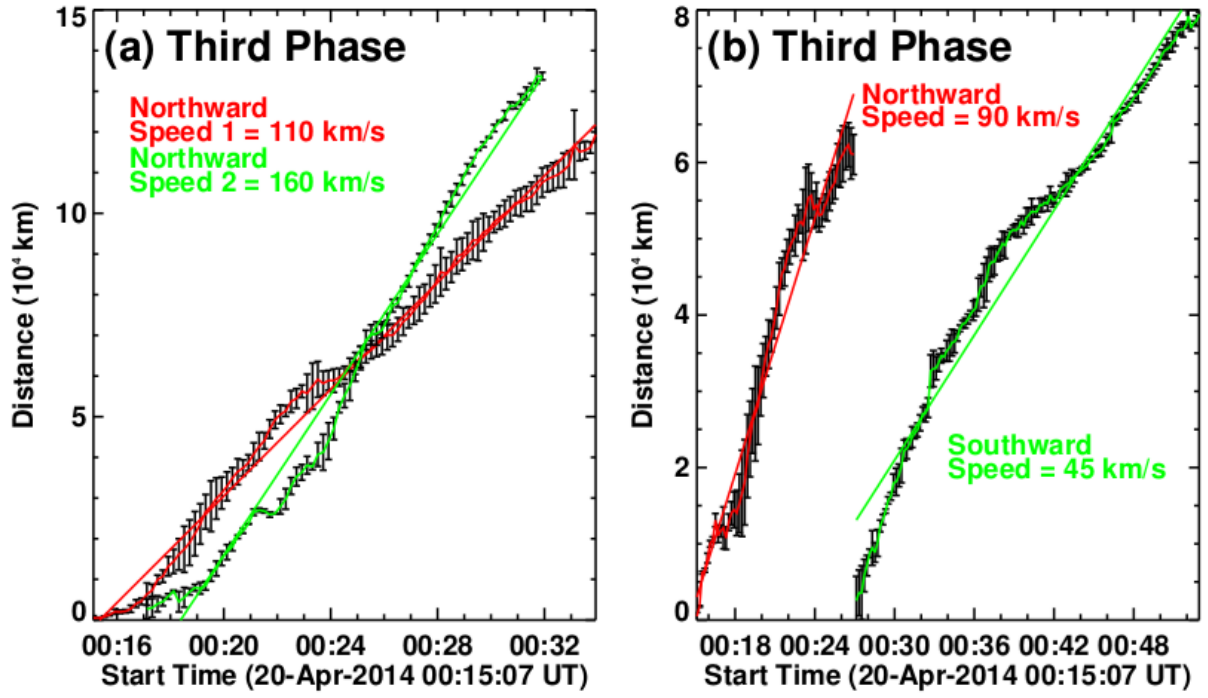


Fig. 11.— (a) Projected distance–time profiles of the plasma flows along the trajectories 1 (red) and 2 (green). (b) The same for the northward (red) and southward (green) plasma flows along the trajectory 3. These measurements have been made using *SDO*/AIA 304 Å images. The rough trajectories 1, 2 (by dotted white lines), and 3 (by dotted black lines) are shown in Figure 9(d). The error bars are the standard deviations estimated using three repeated measurements of the same region. The linear fit method has been used to estimate the average speeds.

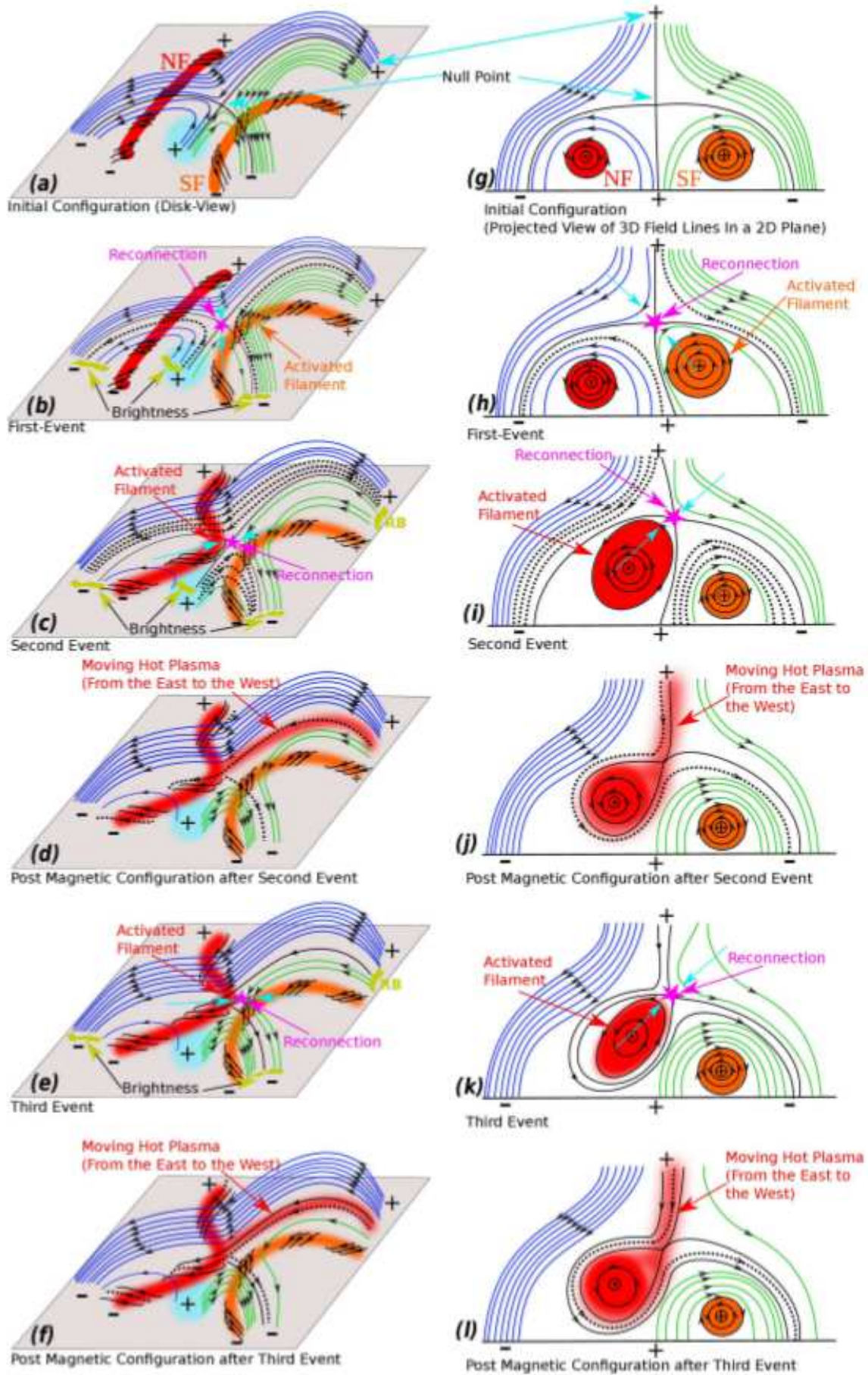


Fig. 12.— Schematic representation of the change in magnetic configuration and the reconnections scenario in the 3D disk view (left column) and projected view of 3D field lines in a 2D plane (right column). The northern (NF) and southern (SF) filaments are shown by the red and orange colors, respectively. Reconnection regions are marked by the pink star, while the reconnected field lines are shown by the dotted black lines. The blue overlying arcades over NF in panels (c), (d), (e) and (f) are not in the plane of reconnection.

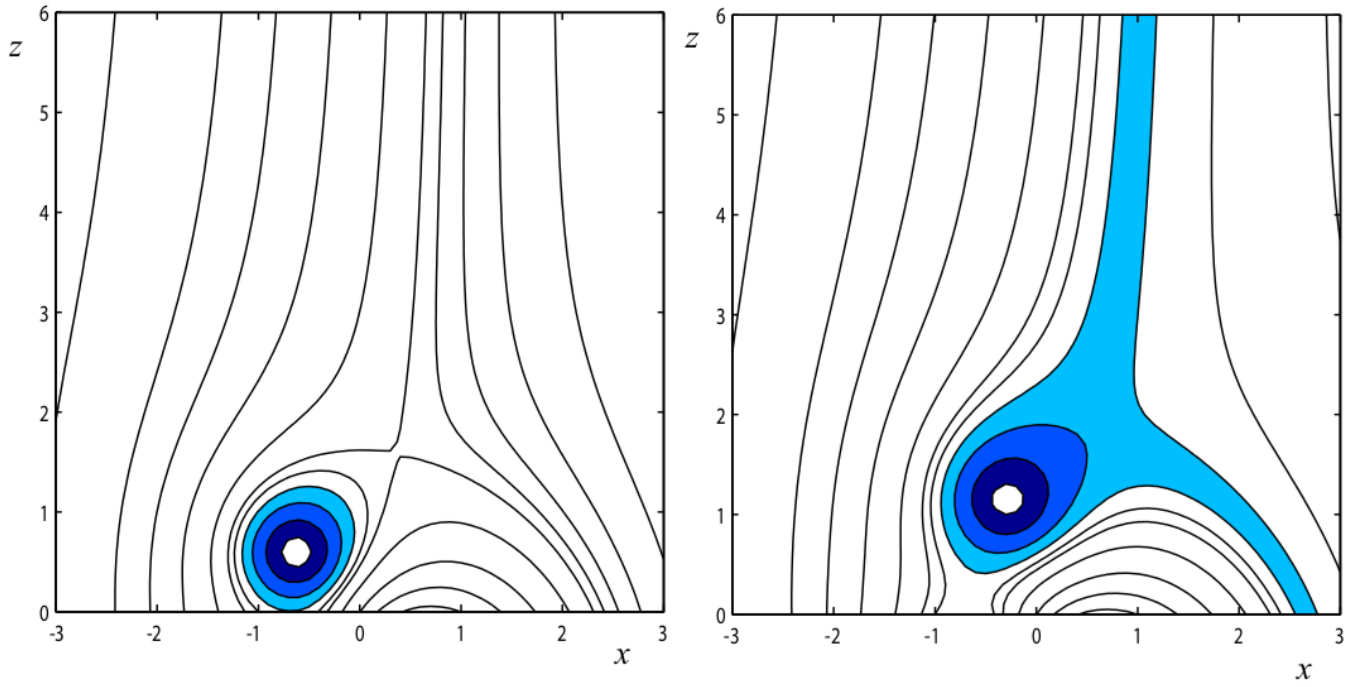


Fig. 13.— 2-D model of the flux-rope magnetic field reconnection at the null point. Black lines represent the magnetic field lines while the different tints of the blue color show the confined plasma.